Applications in Engineering Science 26 (2026) 100332

Contents lists available at ScienceDirect

Applications in Engineering Science

journal homepage: www.elsevier.com/locate/apples

On the use of artificial intelligence and no-tension models in the post-earthquake preliminary assessment of masonry structures

Fernando Fraternali [a],*, Hazar Etteyeb [a], Angela Lato [a], Rana Nazifi Charandabi [b], Mario Spagnuolo [a], Carlo Olivieri [c], Francesco Fabbrocino [c], Angelo Ciaramella [d], Ada Amendola [a]

[a] Department of Civil Engineering, University of Salerno, Fisciano (SA), Italy
[b] Department of Information Engineering, Electrical Engineering and Applied Mathematics, University of Salerno, Fisciano (SA), Italy
[c] Department of Engineering, Pegaso Telematic University, Naples, Italy
[d] Department of Science and Technology, University of Naples Parthenope, Naples, Italy

ARTICLE INFO

Keywords:
Artificial intelligence
Convolutional neural networks
Damage
Earthquakes
Masonry structures

ABSTRACT

This study presents an artificial intelligence-assisted visual inspection procedure and a preliminary resilience assessment technique for the post-earthquake evaluation of masonry structures affected by major Italian earthquakes since 1980. A dataset of 250 images, collected during official surveys conducted by the Italian Civil Protection Department, was analyzed to automatically identify earthquake-induced damage patterns in spatial masonry components. The images, acquired both inside and outside damaged buildings and domed structures, were divided into training, validation, and test sets. The proposed methodology, although still at a preliminary stage due to the limited size of the dataset employed, aims to advance the use of artificial intelligence as a decision-support tool for enhancing structural resilience in post-earthquake scenarios, with particular attention to historic masonry constructions. After training, the AI model achieved a strong ability to correctly identify earthquake-induced damage patterns in masonry structures. The model was also deployed for inference on previously unseen test images, where the predicted bounding boxes qualitatively confirmed its effectiveness in detecting damage patterns. From a mechanical standpoint, the proposed approach supports the formulation of discrete no-tension models for masonry walls and domes affected by seismic events, based on the damage predictions provided by the AI-assisted detection procedure, which are subsequently translated into mechanical representations through engineering-driven post-processing operations. A recently developed strut-and-net approach is then employed to verify the existence of a network of compressed masonry struts capable of sustaining the vertical and horizontal loads acting on the examined structural systems.

1. Introduction

In areas affected by significant earthquakes, there is an urgent need to carry out rapid surveys for the damage assessment of buildings and infrastructures. This is primarily required to determine whether individual buildings can continue to be safely inhabited, as prescribed, for instance, by the Italian Civil Protection through the FAST and AeDES damage survey forms (Baggio et al., 2007, 2014). These investigations are particularly critical in the case of cultural heritage structures, owing to their remarkable historical and architectural value (see Wang et al. (2018), Mishra and Lourenço (2024) and references therein). However, modern buildings also strongly require similar field surveys (De Filippo et al., 2023; Xu et al., 2023; Kumar et al., 2021). In many cases, earthquake-affected areas are dangerous and difficult to access due to the presence of debris on the streets and concerns about structural stability, which calls for the use of drone-assisted image acquisition of damaged buildings (Mishra and Lourenço, 2024).

The use of artificial intelligence (AI) techniques has proven particularly useful when rapid, preliminary information is needed about the damage state of buildings and cultural heritage structures struck by an earthquake and their residual resilience, as demonstrated by several studies available in the literature. One can refer, for instance, to the review papers (Anjum et al., 2024; Li et al., 2025) for an overview of the currently employed approaches, which mainly rely on machine learning (ML) methods and convolutional neural networks (CNNs). To mention just a few examples, these include the binary approach for detecting the complete or incomplete structural state of historical buildings (Muñoz-Silva et al., 2025), the identification of damage types such as cracks, spalling, and efflorescence in historical masonry structures made of

* Corresponding author.
E-mail address: f.fraternali@unisa.it (F. Fraternali).

https://doi.org/10.1016/j.apples.2026.100332
Received 22 April 2026; Received in revised form 25 May 2026; Accepted 26 May 2026
Available online 2 June 2026

bricks (Wang et al., 2018), the visual inspection of earthquake-induced damage (e.g., cracks, spalling, exposure and buckling of reinforcing bars) in reinforced concrete (RC) structures (Xu et al., 2023), as well as AI-assisted detection of damage (cracks, delaminations, stains) on the façades of RC buildings (De Filippo et al., 2023). A rich and insightful literature review of various visual inspection techniques for cultural heritage structures based on AI, machine learning (ML), and computer vision (CV) can be found in Mishra and Lourenço (2024).

The present study introduces an AI-assisted visual inspection procedure and a preliminary stability assessment technique for masonry structures damaged by major earthquake events that have occurred in Italy since 1980, These events include the ‘Irpinia earthquake’ of 23 November 1980 (moment magnitude $M_w = 6.9$); the 1997–1998 ‘Umbria–Marche earthquake’ sequence (maximum magnitude $M_w = 6.0$); the ‘Molise earthquake’ of 31 October 2002 ($M_w = 5.7$); the ‘L’Aquila earthquake’ of 6 April 2009 ($M_w = 6.3$); the ‘Emilia–Romagna earthquake’ of 20 May 2012 ($M_w = 6.1$); and the ‘Norcia earthquake’ of 30 October 2016 ($M_w = 6.3$). An AI-assisted study was conducted using a dataset of 250 photographs personally collected in urban environments affected by earthquakes by one of the authors, Mario Spagnuolo, during his service as a certified technician for the Italian Civil Protection, in which capacity he was responsible for completing the AeDES survey forms pertaining to the aforementioned seismic events. This dataset was processed using Convolutional Neural Network (CNN) -based software developed in collaboration with the partner company (Solomon Technology Corporation, 2025), with the aim of detecting four types of crack damage in stone or brick masonry structures, namely, horizontal, vertical, diagonal, and X-shaped cracks—as well as masonry spalling. The processed images varied in size and were taken at different distances, both outside and inside the examined structures. They were divided into a training set containing 70% of the total images, and validation and test sets each comprising 15%. The training and validation images were manually annotated.

A primary objective of the present study is to provide a practical methodology to support engineers and technicians in the compilation of post earthquake survey forms for damaged buildings and domes, through the use of images acquired from ground-based inspections in accessible areas and/or by unmanned aerial vehicles. In addition, the study investigates the feasibility of predicting the stability of earthquake-damaged masonry buildings and historic heritage structures by means of simplified no-tension models consisting of networks of compressed members (hereafter referred to as strutnet or ‘strutnet’ models), which do not require detailed knowledge of material parameters but rely solely on estimates of the external vertical and horizontal loads. These models, recently proposed for the no-tension analysis of masonry walls and arches (Amendola et al., 2023a,b), explicitly account for the presence of obstacles that cannot be crossed by masonry struts. In the present framework, such obstacles are identified with spalled or cracked masonry regions, as predicted by the AI-assisted damage detection procedure, in accordance with element-erosion approaches to crack damage (Al-Ostaz and Jasiuk, 1997; Schmidt et al., 2009; Pandolfi and Ortiz, 2012). As a consequence, the damaged structure is idealized as an equivalent composite system consisting of undamaged masonry regions and voids.

The proposed framework contributes to the development of intelligent, data-driven tools for rapid structural assessment and decision-making in post-earthquake contexts. By integrating artificial intelligence with sustainability-oriented engineering methods, the study supports the creation of safer, more resilient, and adaptive urban environments, consistent with the broader goals of sustainable reconstruction and risk mitigation in seismic regions. The remainder of this paper is organized as follows. Section 2 introduces the adopted CNN-based methodology, while Sections 3 and 4 describe the image dataset and the performance metrics of the CNN algorithm. Section 5 illustrates the strutnet models developed for benchmark examples of a masonry wall and a masonry dome, which are analyzed through the proposed AI-assisted methodology under combined vertical and horizontal loads. Finally, Section 6 summarizes the main findings of the study and highlights directions for future research.

2. Employed neural-network methodology

This study employs a Neural Network (NN)-based strategy developed through *SolVision*® , an integrated computer-vision platform developed by Solomon Technology Corporation (2025) for high-precision object detection, classification, and measurement. The software combines a suite of advanced deep-learning based approaches with a flexible, project-oriented workflow tailored to support a wide spectrum of industrial inspection and automation tasks. The adopted strategy incorporates multiple NN-based architectures, including YOLO-based detectors, transformer-based models, and proprietary convolutional networks. Depending on the task, users can select from several deep-learning tools – such as Classification, Feature Detection, Instance Segmentation, Instance Keypoint Detection, Optical Character Recognition (OCR), Anomaly Detection, and Feature Matching – each tailored to specific types of visual recognition. The platform also supports multi-stage pipelines through auxiliary tools (e.g., Crop–Rotate, Region Detection, 2D Measurement), enabling hierarchical or multilayer detection strategies.

Model development in *SolVision*® follows an integrated workflow comprising dataset management, manual or semi-automatic annotation, parameter configuration, training, and performance evaluation. The annotation environment supports polygons, masks, keypoints, and automated label generation, while the training interface allows customization of hyperparameters (e.g., learning rate, maximum iteration count, model size) and leverages GPU acceleration via NVIDIA CUDA. A key component of the software is its generative-AI data-augmentation engine, which synthetically expands training datasets through transformations such as histogram equalization, geometric perturbations, viewpoint shifts, noise injection, and background modification. These augmentation strategies increase model robustness under variable environmental and illumination conditions and are complemented by Solomon’s proprietary generative pipelines for producing synthetic training samples—particularly valuable when annotated data are limited. The software further includes a comprehensive analysis module for post-training evaluation, offering confusion-matrix visualization, precision–recall–accuracy metrics, IoU-based validation, misclassification reporting, and interactive score-threshold optimization. *SolVision*® supports real-time inference from multiple cameras, virtual camera streams, or folder-based inputs, and it interfaces seamlessly with industrial systems via TCP/IP or Modbus PLC communication. These interfaces allow the software to transmit detection results, control external devices, or automatically switch among pre-loaded models. Overall, *SolVision*® provides a fully integrated environment for developing and deploying deep-learning vision models. Its modular architecture, support for state-of-the-art algorithms, and extensive augmentation and evaluation capabilities make it particularly well suited for demanding tasks such as defect detection, robotic manipulation, metrology, and automated visual inspection.

3. Illustration of the image dataset

This section presents a selection of images from the database used in this study, documenting earthquake-damaged buildings and domed structures affected by major earthquakes that have occurred in Italy since 1980. As previously mentioned, the dataset used in this study comprises 250 photographs captured by one of the authors, Mario Spagnuolo, during his work as a certified technician for the Italian Civil Protection, where he was tasked with completing AeDES survey forms related to the cited earthquake events. Of these images, 175 (70%) were randomly allocated to the training set, while the validation and testing sets each contained 38 images, corresponding to approximately 15% of the total dataset.

We begin by illustrating the images shown in Fig. 1, which consist of unannotated samples taken from the training dataset. The photograph in Fig. 1(a) shows a two-story building in San Giuliano di Puglia damaged by the 2002 Molise earthquake. The structure did not exhibit a box-like behavior; as a consequence, the masonry piers oscillated asynchronously under the seismic action. The façade wall, in particular, rotated outward toward the street, creating two clearly visible vertical separations on the adjoining wall to which it had been connected. The street-facing wall was especially vulnerable because the ground floor contains several large openings, considerably wider than those on the upper level. Fig. 1(b) illustrates the damage sustained on the ground floor of another building in the same city, also affected by the 2002 Molise earthquake. This structure was built using mixed masonry, with stone blocks alternating with hollow clay bricks, and features large openings at the ground floor. Shear cracks can be observed at the first level, together with some spalling in the areas composed of hollow bricks. Fig. 1(c) illustrates the seismic damage sustained by a relatively new building in the municipality of Novi di Modena during the Emilia–Romagna earthquake. The structure exhibits notable structural deficiencies. The left portion was constructed with a reinforced concrete frame, featuring large ground-floor openings where shop windows were installed, while the right portion consists of load-bearing masonry walls. As a result, there is a pronounced eccentricity between the centers of mass and stiffness, further accentuated by the presence of two stairwells located in the masonry section, both of which experienced significant damage. As expected, the seismic forces produced the most severe effects in the masonry portion of the building. Finally, Fig. 1(d) shows the damage sustained by a building constructed with rubble-filled masonry (muratura a sacco) in the municipality of Preci (Perugia), which was affected by the 2016 Norcia earthquake. The widespread spalling observed on the outer wythe at the corner of the building indicates that the two masonry leaves forming the load-bearing walls did not act together during the seismic event, as they were not properly interconnected.

Fig. 2 shows unannotated images extracted from the validation subset of the photographic database. The case illustrated in Fig. 2(a) refers to shear cracks observed inside a building damaged by the 2012 Emilia–Romagna earthquake, above an opening that had not been reinforced with an adequate lintel. The presence of a floor structure made of wooden beams and hollow bricks can also be observed. Fig. 2(b) shows severe detachment damage affecting the external facing of a portion of the city walls of Norcia, struck by the 2015 earthquake, built in rubble core masonry. Widespread cracking damage is also visible in the same facing. Finally, Fig. 2(c,d) show shear damage in two buildings located in San Giuliano di Puglia, affected by the 2002 Molise earthquake, corresponding to an oblique wall and a front wall, both situated on the ground floor.

Moving on to the figures included in the test subset of the image database, we note that Fig. 3(a,b) illustrate the shear damage observed on the ground floor of the façade of a building located in San Giuliano di Puglia (a), and the similar damage that occurred near a doorway inside another building in the same town (b), both affected by the 2002 Molise earthquake. In Fig. 3(a), one can observe, on the ground floor, very wide openings that are not aligned with those on the upper level, as well as masonry with an irregular texture, consisting of stone portions alternating with sections of hollow brick. A similar type of masonry can be observed in Fig. 3(b), where the collapse of a portion of the floor with brick vaults supported by iron beams above the opening is also evident; this was certainly the cause of the observed shear-related damage.

We conclude with the examination of the spatial domed structure shown in Fig. 3(c–f). This structure covers the central part of the Gasparini Casari chapel, also known as the Oratory of the Immaculate Conception, located in Novi di Modena (MO), in the Sant'Antonio in Mercadello area, on Via Mazzarana (GPS coordinates: 44.8757738, 10.9598901). The chapel was severely affected by the 2012 Emilia–Romagna earthquake. Fig. 4 provides further details concerning the damage observed at the drum of the central dome following the earthquake (panels a,b), as well as exterior views of the chapel before and after the event (panels c,d). The pre-earthquake photograph was kindly provided to Mario Spagnuolo by the owners of Villa Gasparini, in which the chapel is located. Examination of Fig. 4(c,d) reveals that the building underwent several modifications in the years preceding the 2012 earthquake, including the closure of several openings.

Table 1
Training parameters.

Parameter	Result
max dim	640 px
min dim	640 px
max iter	2000
lr	0.01

The most severe damage caused by the 2012 earthquake is concentrated in the drum and is likely attributable to an eccentricity in the closure of the oculi and to the absence of an adequate ring beam. Figs. 3(c,d) and 4(a,b) illustrate the detachment along the edges of several brick infills closing the oculi, together with the absence of an adequate ring beam at the roof level. Finally, Fig. 3(e,f) document the presence of tie rods at the springing of the four arches supporting the weight of the drum, which appear to have prevented its collapse by effectively restraining the supporting base.

4. Assessment of the employed CNN procedure

We present hereafter an assessment of the performance of the employed CNN procedure, based on the *SolVision*® software, in processing the database of earthquake-damaged masonry structures and in developing a prediction model evaluated through the validation and test phases. We begin by analyzing the results presented in Figs. 5, 6, and 7, which display the annotated versions of the images in the training, validation, and test subsets of the database, previously illustrated and discussed in the preceding section.

The *SolVision*® model described in Section 2 was executed using the following training parameters listed in Table 1: *minimum dimension (min dim)* in pixels (px): when the smallest edge of an input image exceeds the defined minimum size, the system scales the image proportionally so that this edge matches the required lower limit, ensuring the image is suitable for the training process; *maximum dimension (max dim)*: once the image has been adjusted to meet the minimum size requirement, a second resize step is applied if its longest side still exceeds the predefined maximum. In this case, the image is scaled down again keeping its aspect ratio intact so that the longest edge conforms to the maximum limit, ensuring its suitability for model training; *maximum iterations (max iter)*: this parameter defines the total number of training cycles the system will execute. Each iteration represents a complete pass through the dataset, meaning the specified value determines how many times the model processes the input images during training; *learning rate (lr)*: this parameter controls the extent to which the model's weights are updated at each training step.

In addition to the previously described training variables, the model employs a set of detection parameters (Table 2) regulating the post-processing of the network outputs and defining the final predictions. Main parameters include: *max_detections* which limits the total number of detected objects; *score threshold*, excluding detections below the confidence limit; *nms_different_class*, which applies non-maximum suppression (NMS) to overlapping objects of different classes, removing the less confident one (range: –1 disables NMS; 0–1 controls suppression strength); and *merge threshold*, which merges overlapping detections of the same class instead of discarding one (range: –1 disables merging; 0–1 adjusts sensitivity to overlap). Beyond the global score threshold, class-specific thresholds were defined to account for differences in visibility and structural importance among damage types: *horizontal,*

Fig. 1. Illustration of various unannotated images included in the employed training dataset. (a,b) City of San Giuliano di Puglia, Molise earthquake: (a) vertical crack causing the separation of two orthogonal masonry walls in a two-story building; (b) combination of horizontal, vertical, and diagonal cracks in the masonry portion (right side) of a mixed reinforced concrete–masonry structure. (c) City of Novi di Modena, Emilia–Romagna earthquake: X-shaped crack on the masonry wall of the right-hand portion of a building constructed in masonry, adjacent to an undamaged section built in reinforced concrete (left side). (d) City of Preci (Perugia), Norcia earthquake: spalling at the intersection of two orthogonal double-leaf masonry walls.

Table 2
Detection parameters.

Parameter	Result
max_detections	100
score threshold	0.1
nms_different_class	−1
merge threshold	0.5
horizontal cracks threshold	0.1
vertical cracks threshold	0.1
diagonal cracks threshold	0.1
X_crack threshold	0.1
spalling threshold	0.1

vertical, diagonal and *X_crack thresholds*; and *spalling threshold*. This configuration balances false positives and negatives, improving both detection precision and operational reliability in post-earthquake masonry inspection.

To enhance the generalization capability of the CNN, a comprehensive *Data Augmentation* pipeline was implemented during training. The adopted augmentation parameters are listed in Table 3. Each image was randomly transformed through a set of controlled geometric and photometric operations designed to replicate the heterogeneity of post-seismic field conditions. The augmentation pipeline included *brightness*, *contrast*, and *saturation* adjustments, as well as the addition of *Gaussian noise* to simulate real environmental variability, and *rotation* to improve orientation invariance. A total of 4000 iterations was selected as an optimal compromise between exposure to diverse augmented samples and computational efficiency. The augmentation process was applied dynamically during training and therefore did not physically increase the size of the stored dataset. Furthermore, the training, validation, and test subsets were generated prior to the augmentation procedure, thereby ensuring the absence of data leakage among the different phases of the CNN evaluation process.

The following results present the performance of the trained *SolVision*® model through a comparison between the *Ground Truth* (GT) annotations and the *Detection Results* (DR). The analysis highlights key performance indicators, including *Precision*, *Recall*, *Accuracy*, *F1-score*, the *Confusion Matrix*, detection line charts, and lists of misclassifications. The main performance metrics of the trained CNN model are summarized in Table 4. Here, *Ground Truth* (GT) denotes the total number of labeled objects in the dataset used during the detection phase, while *Detection* refers to the number of objects identified in

Fig. 2. Illustration of selected images contained in the validation dataset prior to annotation. (a) Crack damage inside a building struck by the 2012 Emilia–Romagna earthquake, visible above an opening lacking a reinforcing lintel; (b) Detection of masonry spalling on the external wall surface and cracking in a section of the city walls of Norcia, damaged by the 2016 earthquake, built with rubble-filled masonry; (c,d) Detection of shear cracking damage in two buildings in the city of San Giuliano di Puglia, struck by the Molise earthquake.

Table 3
Data augmentation parameters applied during CNN training.

Augmentation technique	Type	Percentage
brightness	Photometric	±20%
contrast	Photometric	±20%
saturation	Photometric	±20%
Gaussian noise	Noise	±20%
rotation	Geometric	±10%

the same images. *Precision* is the ratio of correctly predicted positive instances to all instances classified as positive, reflecting the reliability of positive predictions. *Recall* measures the proportion of correctly detected positives relative to all actual positives, indicating the model's sensitivity to true detections. *Accuracy* expresses the overall proportion of correct predictions among all classes and is particularly meaningful when classes have comparable importance. *F1-score* is a harmonic mean of precision and recall that provides a single measure of a classifier's accuracy in balancing false positives and false negatives. The *mean Average Precision* (mAP) quantifies the model's performance on *Regions of Interest* (ROIs), such as object detection, instance segmentation, and keypoint estimation, ranging from 0 to 1, with higher values indicating greater detection precision. Finally, *OKPrecision*, *OKRecall*, and *OKAccuracy* are analogous metrics used for non-ROI tools (e.g., classification or anomaly detection). An image is labeled as *OK* in the ground truth when it contains no NG (No. Good) annotations, and the corresponding detection is *OK* if no NG objects are identified. These adapted metrics evaluate how accurately the model classifies or detects *OK* images independently of ROI-based evaluation.

The loss curve obtained at the end of the training process is shown in Fig. 8, where the X-axis represents the number of training iterations and the Y-axis reports the loss, defined as the objective function minimized during training, which quantifies the discrepancy between the neural network predictions and the corresponding ground-truth annotations.

The Confusion Matrix illustrated in Fig. 9 is derived from the Intersection over Union ('IoU') measure applied to the analyzed images. The IoU, which varies between 0 and 1, quantifies how much the Ground Truth (GT) and the Detection Result ('DR') overlap, and is determined by dividing the area of intersection of the GT and DR by their area of union. An IoU value of 0 signifies that the GT and DR do not intersect at all, whereas a value of 1 indicates a perfect match between them. The confusion matrix displays the names of all damage categories along with the quantitative correspondence between Ground Truth (GT) and

Fig. 3. Illustration of selected images included in the test dataset before the application of the CNN damage-detection procedure. (a,b) Shear damage on the ground floor (a) and in the interior (b) of buildings located in the city of San Giuliano di Puglia, affected by the 2002 Molise earthquake; (c–f) Cracking and spalling damage observed on both the exterior and interior of the Gasparini Casari Chapel, located in the Province of Modena and affected by the Emilia–Romagna earthquake.

Table 4
Performance metrics of the employed *SolVision*® model on the evaluation set.

Metric	Result
Ground Truth	2757
Detection	2393
Precision	0.797
Recall	0.865
Accuracy	0.688
F1-score	0.828
mAP	0.629
OKPrecision	0.797
OKRecall	0.865
OKAccuracy	0.711

Detection Result (DR). Class labels along the horizontal axis represent the detected outputs, while those on the vertical axis correspond to the actual GT labels. Accurate classifications appear along the diagonal extending from the top-left to the bottom-right of the matrix. The value shown in the 'Remain' row indicates the number of detected objects whose IoU value falls below the threshold defined in the system (IoU < 0.1). Conversely, the 'Repeat' field shows the cases where multiple detections correspond to the same GT object. In such instances, only the detection with the highest IoU is considered True, whereas the remaining overlapping detections are marked as False (repeated).

By examining the confusion matrix, we observe that the CNN effectively prioritizes the key visual features associated with the different classes of masonry damage, despite the relatively small number of images constituting the examined dataset. Strong diagonal activations, especially for Spall (216 TP) and Vertical crack (202 TP), show high reliability in detecting pronounced material discontinuities (with TP denoting True Positive). The network also performs well on Diagonal crack (141 TP) and Horizontal crack instances, confirming that its multi-scale architecture successfully captures multiple crack orientations and aligns convolutional filters with the dominant propagation patterns observed in masonry under lateral or shear loads. Cases labeled Remain, characterized by IoU values slightly below the threshold, indicate that the model still localizes damaged regions even when fracture profiles are fragmented or partially degraded—an ability typical

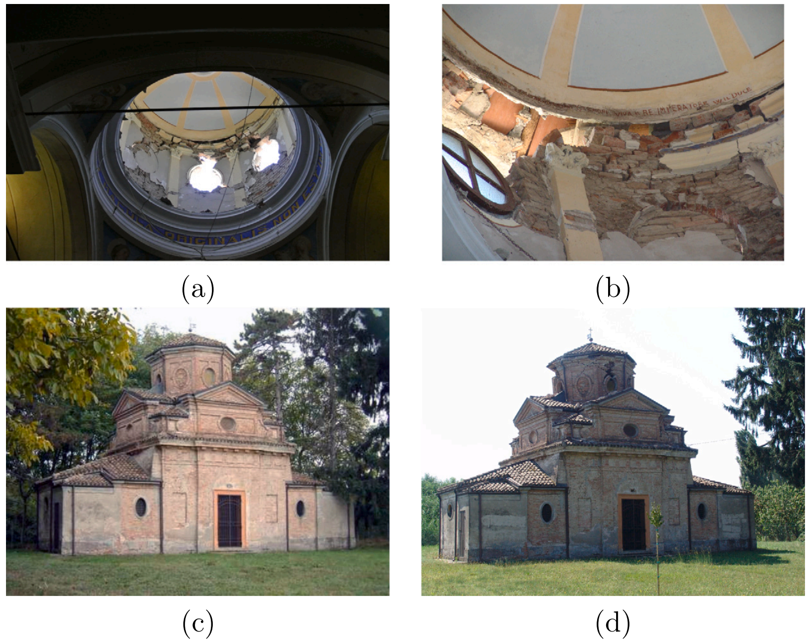

Fig. 4. (a, b) Additional images illustrating the damage observed at the drum of the dome of the Gasparini Casari chapel. (c, d) Exterior views of the chapel before (c) and after (d) the 2012 Emilia–Romagna earthquake.

of focus-aware segmentation with deformable kernels. The near-zero Repeat count further demonstrates stable one-to-one correspondence between detected regions and their associated masks, reflecting effective suppression of duplicate proposals. Overall, the confusion matrix highlights a balanced integration of architectural depth, spatial feature concentration, and domain-specific learning. The trained model exhibits a clear structural understanding of post-earthquake degradation patterns, consistent with both the mechanics of masonry failure and current state-of-the-art deep instance segmentation performance.

As regards the performance metrics reported in Table 4, the employed CNN procedure achieves an F1-score of 0.828, a value substantially higher than the 0.685 reported in Pantoja-Rosero et al. (2022) for a dataset of 162 images of damaged buildings in the 'wild' (i.e., stone masonry structures affected by real earthquakes and photographed in urban environments). This comparison is particularly significant, as the study by Pantoja-Rosero et al. like the present work, examines complex crack patterns rather than merely detecting whether cracks are present. The measured Accuracy of 0.688 is lower than the values reported in Reis and Khoshelham (2021), Pratibha et al. (2023), Ravichand et al. (2022), Katsigiannis et al. (2023), which approach or exceed 90% for the simpler binary task of detecting the presence or absence of cracks. This gap is expected, since the present methodology does not simply flag damage but instead classifies crack-related deterioration into four distinct categories (horizontal, vertical, diagonal, and X-shaped cracks), a substantially more demanding problem.

5. No-tension modeling of damaged masonry structures

The mechanical modeling of masonry structures presents significant challenges due to several factors, including the material's intrinsic inhomogeneity and nonlinear behavior, the wide variability in the texture of bricks and stones, and the ageing effects commonly observed in historical constructions, to mention only a few (see, e.g., Como (2013), Angelillo (2014) and references therein). A simple mechanical model suitable for a first-approximation (preliminary) safety assessment of earthquake-damaged structures is the Rigid No-Tension (RNT) model. This model represents masonry as a rigid, homogeneous, unilateral material that does not resist tension under external loading and is assumed to possess infinitely large compressive strength (Como, 2013; Angelillo, 2014; Heyman, 1995). It is particularly useful when no reliable information is available on the actual material parameters of masonry. However, the RNT model can be effectively employed within a limit analysis framework (Amendola et al., 2023a) only when a rocking-type collapse mechanism is expected to precede shear failure, a condition frequently observed in historical masonry constructions (Como, 2013). A comprehensive stability assessment of a masonry construction, nonetheless, requires comparing the predictions of the RNT model with those obtained from more complex mechanical formulations. These formulations should account for shear damage (Bagi, 2014; Beatini et al., 2019), finite compressive strength, and should incorporate texture information together with experimental data from material and component tests conducted in structural laboratories. The proposed framework establishes a preliminary conceptual bridge between AI-assisted damage detection and simplified no-tension mechanical modeling. At the present stage, the transition from the CNN outputs to the mechanical interpretation of the damaged regions relies on engineering-driven post-processing, whereby the detected cracks and spalled areas are represented as equivalent obstacles within the strut-net formulation.

Fig. 10 illustrates the reference scheme for masonry crack patterns provided in the AeDES Manual of the Italian Civil Protection (Baggio et al., 2014), together with a description of the main types of damage typically observed in masonry buildings after an earthquake. These include: nearly vertical cracks above the lintels of openings; diagonal cracks in spandrel zones (window sills and lintels); diagonal cracks in vertical elements (piers or wall panels); local crushing of masonry, with or without material spalling; nearly horizontal cracks at the top and/or bottom of wall piers; nearly vertical and through cracks at wall intersections; spalling of masonry at beam supports due to pounding effects; formation of a displaced wedge at the junction of two perpendicular walls; failure of tie rods or pull-out of their anchorages; horizontal cracks at floor or roof levels; and detachment of one wythe in double-leaf walls.

Recent studies have introduced a strutnet approach for the rigid no-tension (RNT) modeling of masonry structures (Amendola et al., 2023a,b). To verify whether a planar RNT structure fixed at r points (the reactive points') can sustain a prescribed set of external forces applied at n points (the active points'), it is assumed that such forces

Fig. 5. Training phase: annotation of the images shown in Fig. 1. In this and the following figures, the defined damage classes include vertical, horizontal, diagonal, and X-shaped cracks, as well as masonry spalling, represented by the color codes displayed at the top of the figure.

are distributed along the boundary of a convex region Ω. The boundary points, denoted $\mathbf{x}_1, \mathbf{x}_2, \ldots, \mathbf{x}_N$ with $N = n + r$, are indexed counterclockwise. Smooth force distributions or extended attachment areas may be represented through an appropriate discretization. The formulation also allows for the presence of convex polygonal subregions $O_1, \ldots, O_s \subset \Omega$ that cannot sustain any stress, for instance because the structure contains a hole or is locally damaged. These subregions act as voids which, together with the surrounding undamaged masonry, define an equivalent composite system of the masonry structure. The forces applied at the active points consist of fixed vertical forces $\mathbf{g}_i$ and horizontal forces $\mathbf{q}_i$, scaled by a horizontal force multiplier λ, which can be interpreted as a rough estimate of the spectral acceleration associated with an equivalent static seismic loading of the wall (Bourahla, 2013).

The stress distribution is governed by an Airy stress function ϕ. The strutnet approach consists in assuming that this function is piecewise linear. The RNT condition is enforced by requiring ϕ to be concave. Consequently, ϕ can be written in the form $\phi = \min_j L_j$, where each L_j denotes a linear function. The gradient $\nabla\phi$ is therefore piecewise constant, and the corresponding stress field, interpreted in the sense of distributions, is a measure supported along the jump lines,referred to as ‘struts’, of $\nabla\phi$. One may alternatively visualize the graph of ϕ in $\mathbb{R}^3$, which is piecewise planar and convex, resembling a roof. The horizontal projections of the edges formed by the intersections of adjacent planar facets correspond to the struts where the stress is concentrated. As no external force is applied between points x_i and x_{i+1}, a single linear function, denoted L_i, coincides with ϕ along that boundary segment. Consequently, equilibrium with the external forces requires that, for any active point x_i, the following condition holds

$$\mathbf{R}_\perp(\nabla L_{i+1} - \nabla L_i) = -(\mathbf{g}_i + \lambda \mathbf{q}_i), \quad i = 1, 2, \ldots, n, \tag{1}$$

where $\mathbf{R}_\perp$ is a 90° rotation (Amendola et al., 2023b). The concavity of ϕ imposes, for all i and j in $\{1, \ldots, N\}$

$$L_i(x_j) \geq L_j(x_j) \tag{2}$$

One may also attempt to force the strutnet to remain outside the regions O_q $(q = 1, 2, \ldots, s)$ by requiring the Airy function to be linear over each of these subdomains. This is feasible if and only if there exist linear functions L_{N+q} such that, for every $j \in 1, \ldots, N + s$, $L_{N+q} \leq L_j$

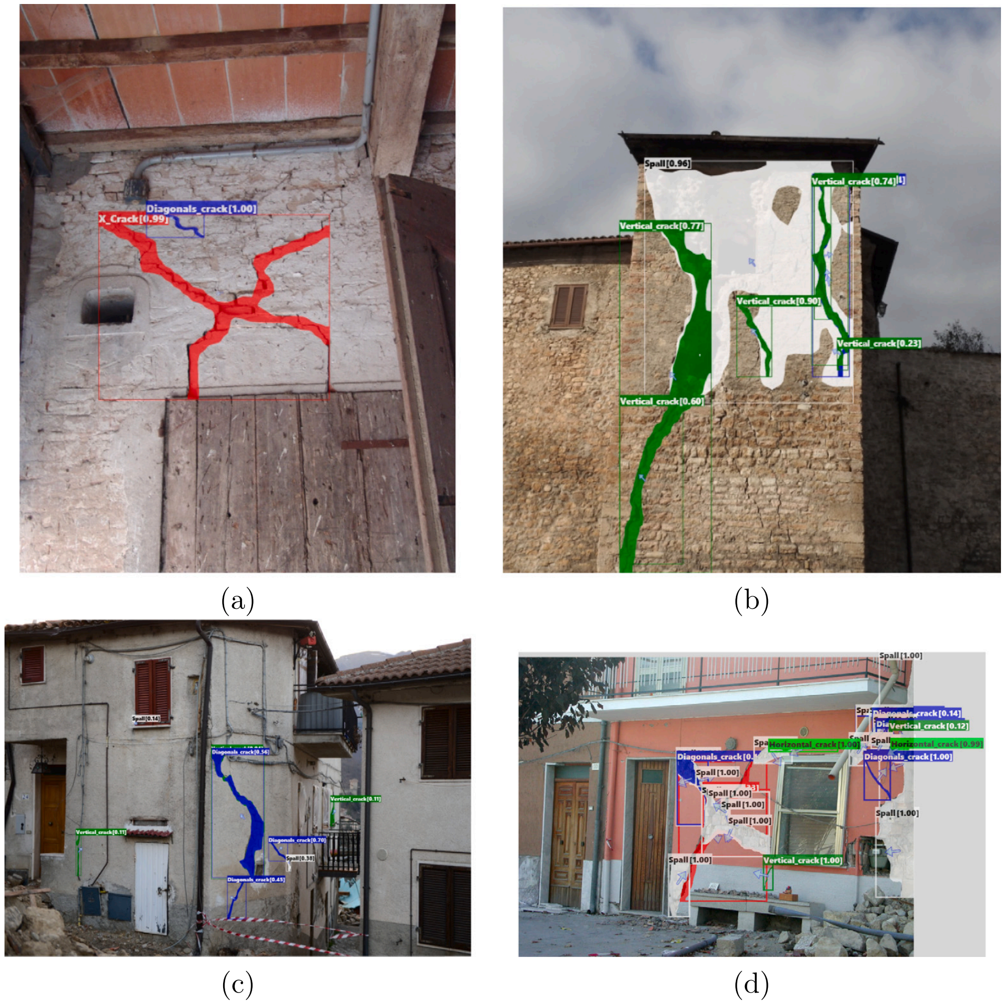

Fig. 6. Validation phase: detection of damage in the images shown in Fig. 2.

on O_q, and such that, for all $i \in 1, \ldots, N$, it results in

$$L_{N+q}(x_i) \geq L_i(x_i) \tag{3}$$

As O_q is assumed to be a convex polygon (convex envelop of $y_1^q, \ldots, y_2^q, y_{n_q}^q$), the condition $L_{N+q} \leq L_j$ on the region O_q reads, for all y_p^q, $p \in \{1, \ldots, n_p\}$

$$L_{N+q}(y_p^q) \leq L_j(y_p^q) \tag{4}$$

If, for the prescribed forces and a given load amplitude λ, we can identify functions L_i satisfying, Eqs. (1)–(4), then an RNT solution exists and the masonry structure under consideration is stable. The set of values of λ for which such a solution exists is, when non-empty, a closed interval $(\lambda^-_{\text{lim}}, \lambda^+_{\text{lim}})$ where λ^-_{lim} and λ^+_{lim} denote the lower and upper 'limit load' multipliers, respectively. The strutnets corresponding to these extreme multipliers are termed the 'limit load strutnets' We refer the reader to Amendola et al. (2023a,b) for a comprehensive exposition of the strut-net methodology, which lends itself to an efficient implementation through a linear programming algorithm tailored to the limit-analysis problem at hand. By employing such an algorithm, we computed the limit-load multiplier for a masonry wall and a masonry dome examined during the test phase of the AI-assisted damage-detection procedure, under two distinct loading conditions: horizontal forces acting from right to left (denoted as $\lambda_{\text{lim}} = \lambda^+_{\text{lim}}$) and from left to right (denoted as $\lambda_{\text{lim}} = \lambda^-_{\text{lim}}$). Since the direction of the applied horizontal force is reversed between the two cases, both multipliers take positive values. The damaged regions corresponding to detachment fractures (Angelillo, 2014), identified by this procedure, are modeled as obstacles, in accordance with the element erosion approach to fracture damage (Schmidt et al., 2009; Pandolfi and Ortiz, 2012). Similarly, the spalled areas detected by the AI-assisted procedure are also represented as obstacles.

5.1. A strutnet model of a damaged building wall

We begin by applying the strutnet algorithm to the limit analysis of a selected building façade examined through the AI-assisted damage-detection procedure. The examined case refers to the first-story portion of the façade analyzed through the AI-assisted damage detection process, as shown in Fig. 7(a). Ten equally spaced active points ($n = 10$) were defined along the top edge of the boundary, together with ten reactive points placed along the bottom edge of each of the three masonry piers forming the wall. We assume that the failure of the examined façade wall may occur through a local collapse mechanism at the ground floor, due to the presence of large openings at this level that are not vertically aligned with those on the upper stories (Como, 2013), as well as the presence of pronounced X-shaped cracks observed in the masonry piers at the same level (see Figs. 3(a), 7(a)). Since our goal is to obtain a first-approximation estimate of the residual horizontal load-carrying capacity of the damaged wall, the analysis focuses on the ratio between the applied vertical and horizontal forces, rather than their absolute values. Accordingly, for the sake of simplicity, all vertical forces $\mathbf{g}_i$ applied to the intermediate nodes along the upper edge of the first-story wall were assigned a unit

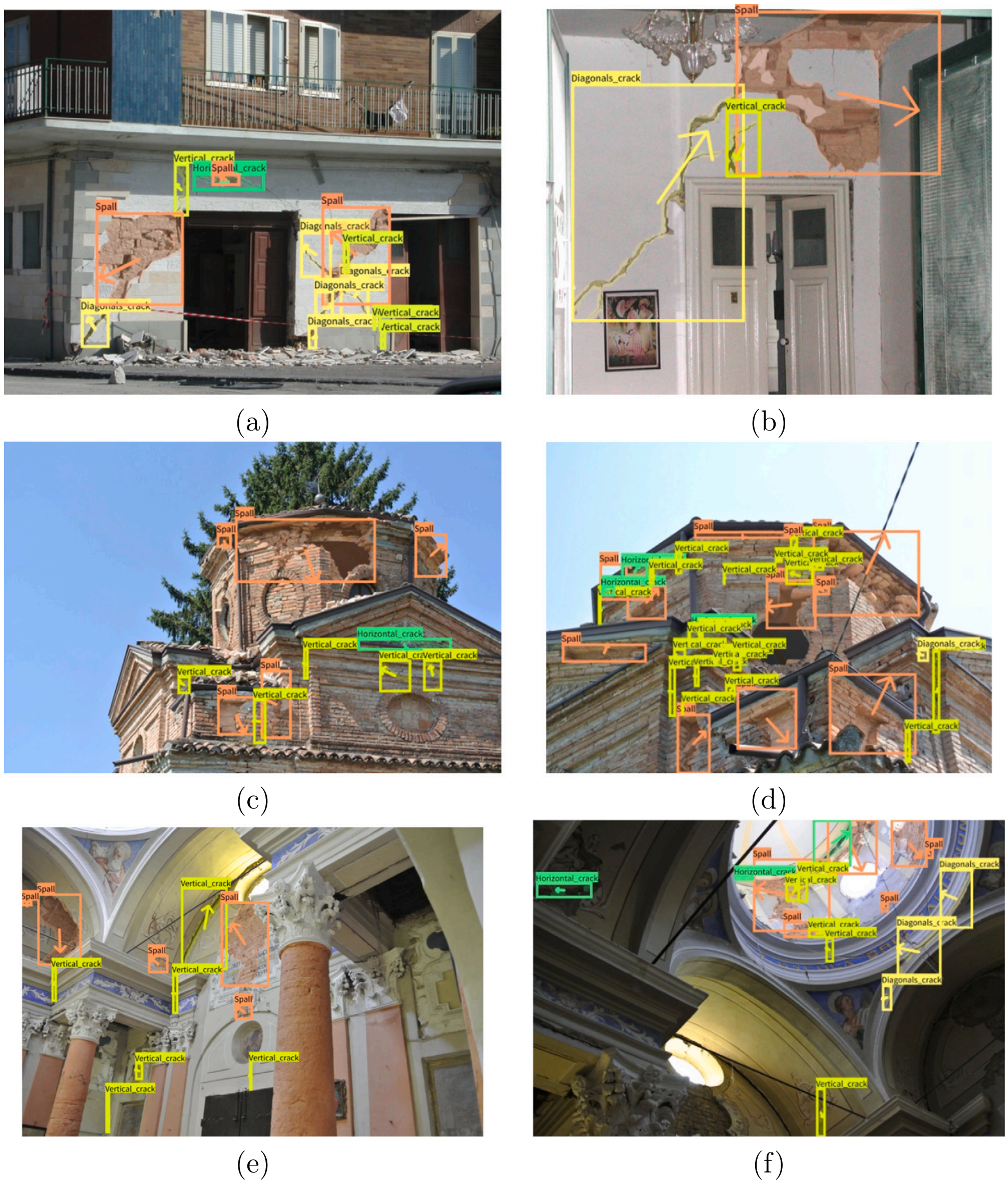

Fig. 7. Test phase: detection of damage in the images shown in Fig. 3.

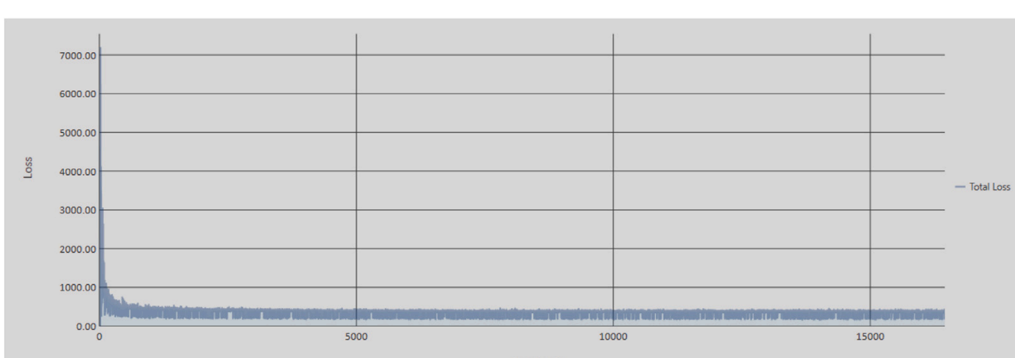

Fig. 8. Loss curve of the employed CNN model, showing the evolution of the loss function as a function of the training iterations..

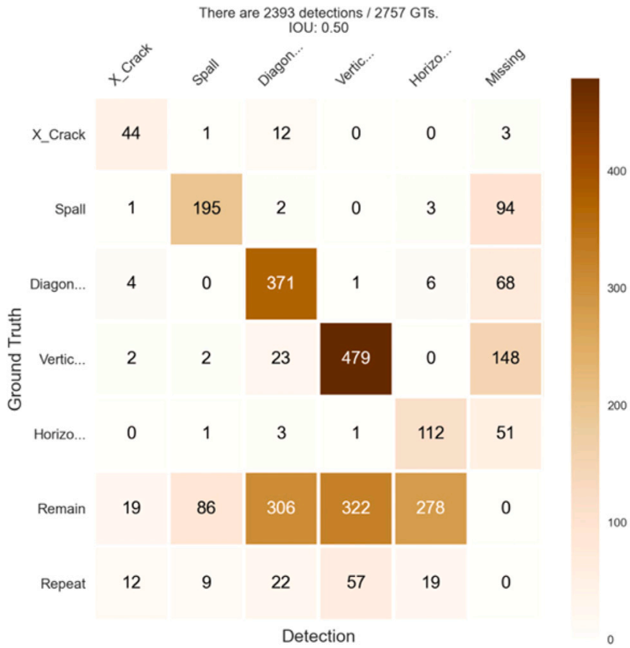

Fig. 9. Confusion matrix of the employed model.

magnitude (in arbitrary units), while the corner nodes were assigned forces of half that value. The horizontal forces were instead lumped into a single resultant $\mathbf{Q} = \lambda_{\text{lim}} \sum_{i=1}^{n} |\mathbf{g}_i|$, applied either at the top-right or top-left corner of the wall. As anticipated, this configuration allows estimation of the residual seismic load-carrying capacity of the wall for horizontal actions directed from right to left ($\lambda_{\text{lim}} = \lambda_{\text{lim}}^{+}$) and from left to right ($\lambda_{\text{lim}} = \lambda_{\text{lim}}^{-}$), respectively.

We examined an undamaged model of the wall and two damaged models, as illustrated in Fig. 11. The analyzed obstacles correspond to the detached portions of the cracks detected in Fig. 7(a), as well as to the door openings at the ground floor. The two damaged models differ from each other, because in the second one we assumed a larger extension of the detachment fractures compared with the first model. In other words, the additional obstacles shown in Fig. 11 were assumed to correspond to superficial cracks in the first damaged model, which do not compromise the local stress-absorption capacity of the masonry.

Fig. 12 illustrates the limit-load strutnets obtained for this example, corresponding to $\lambda_{\text{lim}}^{+} = 0.4766$ and $\lambda_{\text{lim}}^{-} = 0.2942$ for the first damaged model, and to $\lambda_{\text{lim}}^{+} = 0.3616$ and $\lambda_{\text{lim}}^{-} = 0.2145$ for the second damaged model. It is worth noting that for the undamaged model we estimated noticeably higher values of the limit-load multipliers, namely $\lambda_{\text{lim}}^{0,+} = 0.6826$ and $\lambda_{\text{lim}}^{0,-} = 0.3531$. Such results indicate that the examined wall possesses a considerably larger horizontal load-carrying capacity for forces directed from right to left, due to the unsymmetrical arrangement of the openings and the observed damage. Our simplified limit-load analysis therefore leads us to conclude that the post-earthquake damage caused a reduction of approximately 30% in the horizontal load-carrying capacity of the wall for the first damaged model, and on the order of 47% for the second damaged model.

5.2. The case of a damaged dome

We now turn to the analysis of a spatial domed structure examined through the AI-assisted damage-detection procedure. The case under consideration concerns the Gasparini Casari Chapel, previously reported to have sustained severe damage during the 2012 Emilia–Romagna earthquake, as illustrated in Figs. 3(c–f), 4(a,b), and 7(c–f). Section 3 indicated that the most significant damage affecting the structure under examination was concentrated in correspondence with the connection between the dome and the lower supporting elements (i.e., at the dome drum, see Fig. 4(a–b)). It is known that a masonry dome affected by a diffuse meridian crack loses its initial membrane equilibrium, as the hoop stresses carried by the concentric rings in the undamaged state are disrupted. The structure consequently tends to behave as a collection of slices, each forming a pair of semi-arches leaning against one another (see, e.g., Como (2013), Heyman (1995)). Based on this observation, we present below a no-tension model of a slice of the central dome of the Gasparini Casari Chapel, represented as a sector of a spherical arch. Fig. 13 illustrates the geometry of the adopted model, constructed by combining two of the eight semi-arches into which the dome may be subdivided (Fig. 3(c,d)). The thickness of the dome was assumed to be approximately 1.50 m for the purposes of the numerical simulations, as this parameter was not available at the time of the on-site survey. The arch under consideration is subjected to nineteen active vertical forces of unit magnitude applied at the extrados and uniformly distributed along the horizontal projection of the dome, as well as to a central horizontal force of magnitude $\mathbf{Q} = \lambda_{\text{lim}}\mathbf{G}$, where $\mathbf{G}$ denotes the resultant of the vertical forces acting on all dome slices. This modeling choice entails the conservative assumption that the entire seismic load acting in the plane of the arch is resisted solely by such a structural portion, without any contribution from the remaining arches. We examined both an undamaged model of the dome and a symmetrically damaged configuration in which the macroscopic cracks observed at the base of the structure are conservatively extended toward the crown, assuming that the deterioration compromises the masonry in the region immediately adjacent to the intrados. The resulting limit-load strutnets are shown in Fig. 14(a–d). The computed values $\lambda_{\text{lim}}^{+} = \lambda_{\text{lim}}^{-} = 0.044$ and $\lambda_{\text{lim}}^{0,+} = \lambda_{\text{lim}}^{0,-} = 0.170$ indicate that the damaged dome preserves only a markedly reduced horizontal load-carrying capacity, diminished by approximately 74% relative to the undamaged configuration. Due to the very low value of the limit-load multiplier for the damaged model, the strutnets corresponding to forces applied from left to right and from right to left, which are shown in Fig. 14(c–d), are practically coincident.

6. Concluding remarks

This work presented the application of an AI-assisted damage-detection procedure for the preliminary vulnerability assessment of masonry structures affected by earthquakes. The adopted CNN enabled the identification of masonry spalling and four distinct crack-damage typologies from images acquired in real urban environments and at varying distances from the inspected structures. The procedure exhibited satisfactory performance metrics despite the limited size of the employed image dataset, particularly when compared with studies conducted under similar operating conditions (Pantoja-Rosero et al., 2022). The obtained results demonstrated a recall of approximately 86.7% after training, while the inference performed on previously unseen test images qualitatively confirmed the effectiveness of the proposed framework in detecting earthquake-induced damage patterns through the generated bounding boxes. The damage-detection results obtained through the CNN-based procedure were subsequently employed to construct no-tension mechanical models of two benchmark cases, namely a façade and a domed structure, by means of a strutnet approach representing the damaged portions of the construction as mechanically non-resistant regions (Amendola et al., 2023a,b). Such models enabled approximate estimates of the residual seismic load-carrying capacity of the damaged structures, thereby supporting a preliminary assessment of structural stability under post-earthquake conditions.

The present study should be regarded as a proof-of-concept investigation aimed at assessing the feasibility of combining AI-assisted visual inspection with simplified no-tension mechanical models within an integrated post-earthquake assessment framework. At the present

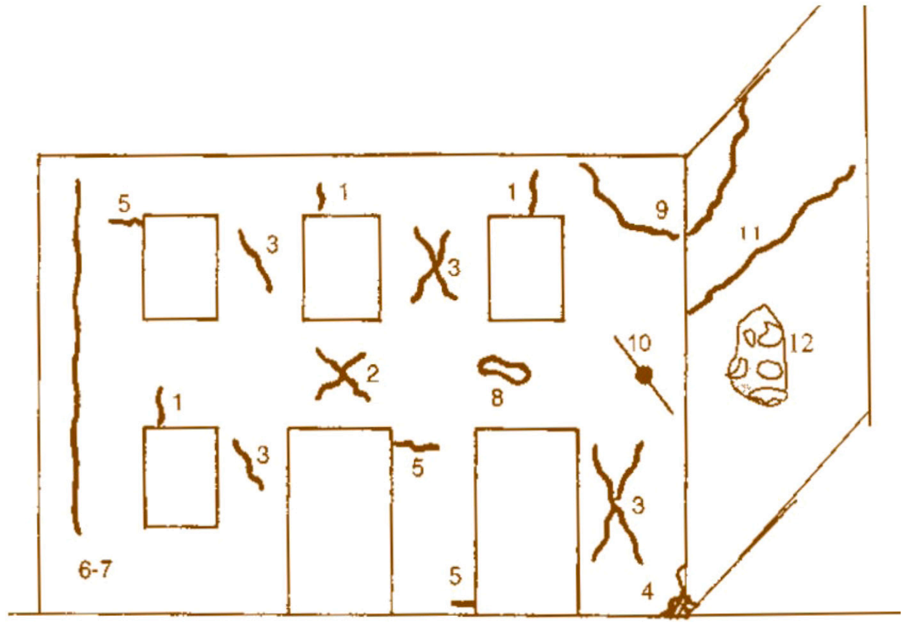

Fig. 10. Typologies of damage in masonry structures as described in the AeDES Manual of the Italian Civil Protection: (1) nearly vertical cracks above the lintels of openings; (2) diagonal cracks in spandrel zones (window sills and lintels); (3) diagonal cracks in vertical elements (piers or wall panels); (4) local crushing of masonry, with or without material spalling; (5) nearly horizontal cracks at the top and/or bottom of wall piers; (6) nearly vertical cracks at wall intersections; (7) through cracks at wall intersections (as in case 6); (8) spalling of masonry at beam supports due to pounding effects; (9) formation of a displaced wedge at the junction of two perpendicular walls; (10) failure of tie rods or pull-out of their anchorages; (11) horizontal cracks at floor or roof levels; and (12) detachment of one wythe in double-leaf walls.
Source: Reproduced from page 54 of Baggio et al. (2014) with permission of the Italian Dipartimento della Protezione Civile – Presidenza del Consiglio dei Ministri.

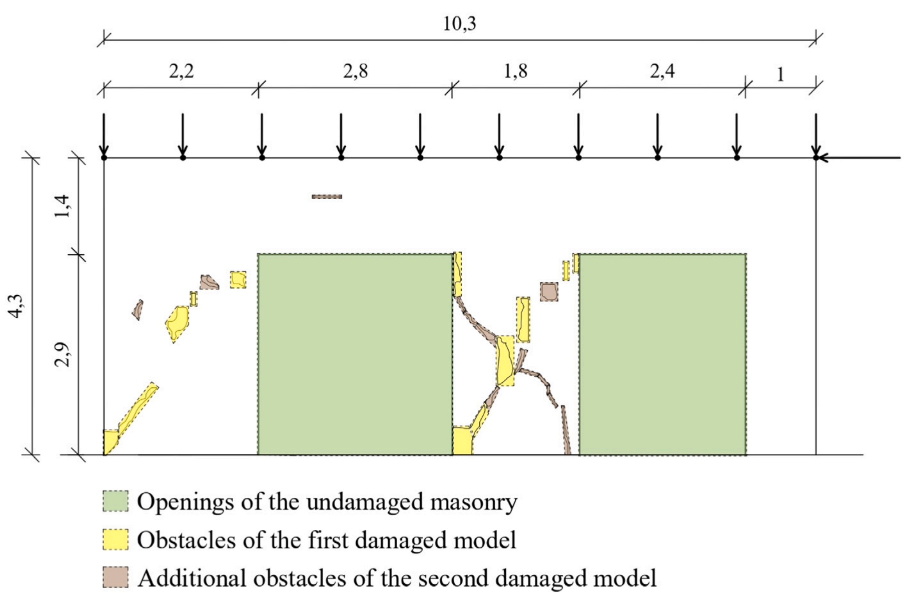

Fig. 11. Geometry and loading scheme of a damaged masonry wall (dimensions in meters).

stage, the transition from the CNN output to the mechanical model still involves an engineering interpretation of the detected damaged regions, which are represented as mechanically non-resistant obstacles within the adopted strut-net formulation. Despite its preliminary nature, the proposed methodology highlights the potential of combining machine-learning tools with mechanically informed structural idealizations to provide rapid and reasonably reliable evaluations of damaged masonry constructions. Such an approach appears particularly promising for the analysis of ordinary and heritage masonry structures, which constitute a substantial portion of the built environment and cultural heritage in Italy and in many other countries worldwide.

Future developments will focus on enlarging and diversifying the image dataset, implementing additional statistical validation strategies, including cross-validation procedures, and improving the generalization capability of the adopted CNN framework. Further efforts will also address the development of more automated CAD-based workflows linking AI-based damage detection to mechanical modeling, as well as the integration of multiscale damage-detection strategies capable of capturing both diffuse and localized degradation phenomena. Parallel

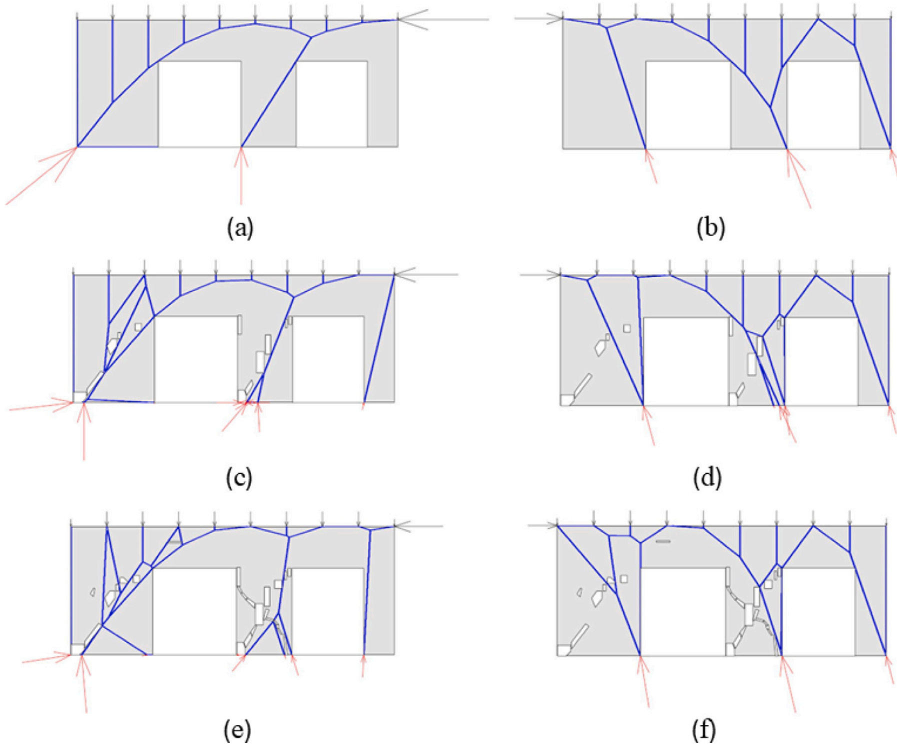

Fig. 12. Limit-load strutnets for the masonry wall example: (a, b) undamaged wall under seismic forces directed from right to left (a: $\lambda_{\text{lim}}^{0,+} = 0.6826$) and from left to right (b: $\lambda_{\text{lim}}^{0,-} = 0.3531$); (c, d) first damaged wall model (c: $\lambda_{\text{lim}}^{+} = 0.4766$; d: $\lambda_{\text{lim}}^{-} = 0.2942$); (e, f) second damaged wall model (e: $\lambda_{\text{lim}}^{+} = 0.3616$; f: $\lambda_{\text{lim}}^{-} = 0.2145$).

investigations will concentrate on the refinement and validation of the adopted no-tension mechanical models through comparisons with advanced nonlinear finite-element and discrete-element approaches, together with experimental benchmark studies. These developments are expected to enhance the robustness, reliability, and applicability of fast AI-supported procedures for post-earthquake structural assessment.

CRediT authorship contribution statement

Fernando Fraternali: Writing – review & editing, Writing – original draft, Visualization, Validation, Supervision, Software, Resources, Project administration, Methodology, Investigation, Funding acquisition, Formal analysis, Data curation, Conceptualization. **Hazar Etteyeb:** Writing – review & editing, Writing – original draft, Visualization, Validation, Supervision, Software, Resources, Methodology, Investigation, Formal analysis, Data curation, Conceptualization. **Angela Lato:** Writing – review & editing, Writing – original draft, Visualization, Validation, Supervision, Software, Resources, Methodology, Investigation, Formal analysis, Data curation, Conceptualization. **Rana Nazifi Charandabi:** Writing – review & editing, Writing – original draft, Visualization, Validation, Supervision, Methodology, Formal analysis, Data curation, Conceptualization. **Mario Spagnuolo:** Writing – review & editing, Writing – original draft, Visualization, Validation, Resources, Project administration, Investigation, Formal analysis, Data curation. **Carlo Olivieri:** Writing – review & editing, Writing – original draft, Visualization, Validation, Methodology, Formal analysis. **Francesco Fabbrocino:** Writing – review & editing, Writing – original draft, Visualization, Validation, Methodology, Formal analysis. **Angelo Ciaramella:** Writing – review & editing, Writing – original draft, Visualization, Validation, Supervision, Software, Resources, Project administration, Methodology, Investigation, Formal analysis, Data curation, Conceptualization. **Ada Amendola:** Writing – review & editing, Writing – original draft, Visualization, Validation, Supervision, Software, Resources, Project administration, Methodology, Investigation, Funding acquisition, Formal analysis, Data curation, Conceptualization.

Funding

This work was supported by the Italian Ministry of University and Research (MUR), Italy under the FIS3 Project "TEnsegrity eXtra tunable metaMATerials (TEXMAT)" (Project Code: FIS-2024-00389, PI: Ada Amendola). F.F. acknowledges the financial support provided by the Italian Ministry of University and Research (MUR), Italy under the project "Fragility, Marginality, Mobility, Energy Transition (FraMMET)" (Project Code: TNE-00074), within the framework of the Italian National Recovery and Resilience Plan (PNRR) – Mission 4 – Component 1 "Enhancement of education services: from nursery schools to universities" – Investment 3.4 "Advanced university teaching and skills", Subinvestment T4 "Transnational initiatives in education", funded by the European Union – NextGenerationEU.

Declaration of competing interest

The authors declare that they have no known competing financial interests or personal relationships that could have appeared to influence the work reported in this paper.

Acknowledgments

The authors thank Solomon® Technology Corporation for the valuable assistance and support provided in the use of the software. They also gratefully acknowledge the collaboration of Raffaele Silvestri and Giuseppe Forino (Department of Civil Engineering, University of Salerno) in the annotation of the image dataset. Finally, the authors express their sincere gratitude to Professor Pierre Seppecher (Institut de Mathématiques de Toulon, Université de Toulon, France) for his remarkable support in adapting the strutnet approach to the present problem.

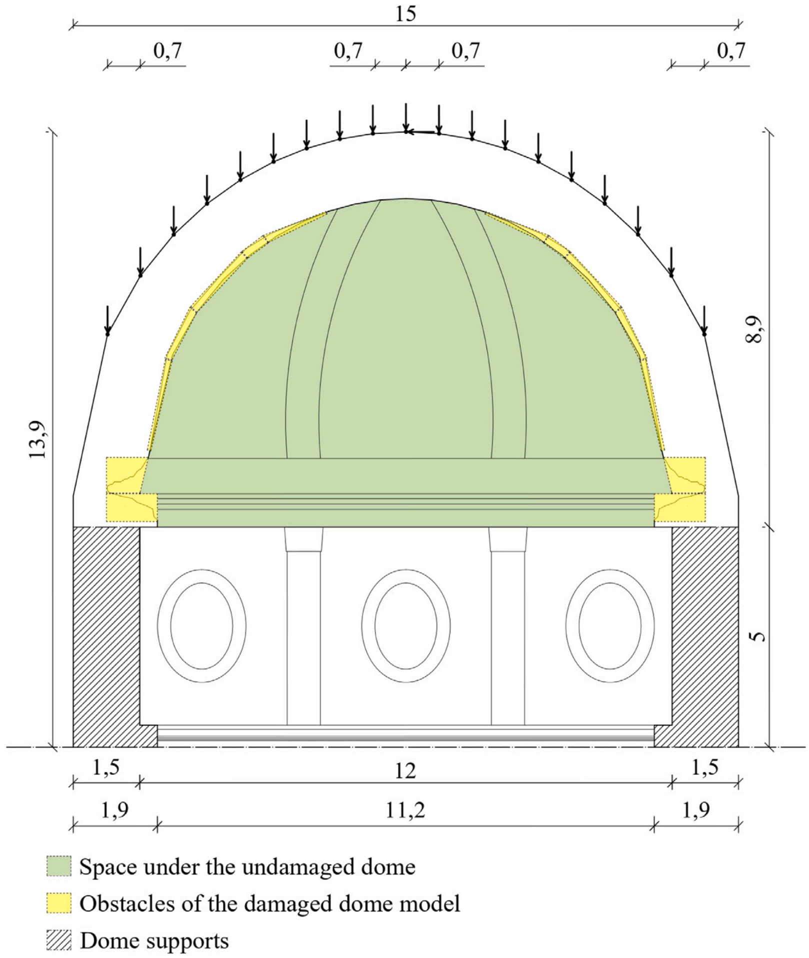

Fig. 13. Geometry and loading scheme of the central dome of the Gasperini Casari Chapel (dimensions in meters).

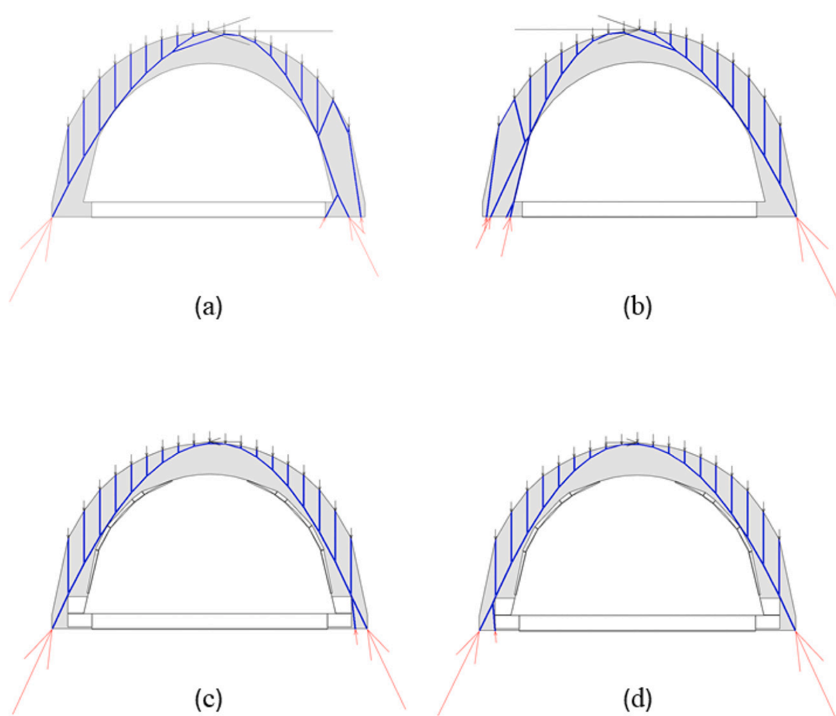

Fig. 14. Limit-load strutnets for the central dome of the Gasperini Casari Chapel: (a, b) undamaged dome under seismic forces: $\lambda_{\mathrm{lim}}^{0,+} = \lambda_{\mathrm{lim}}^{0,-} = 0.170$; (c, d) damaged dome model under seismic forces: $\lambda_{\mathrm{lim}}^{+} = \lambda_{\mathrm{lim}}^{-} = 0.044$.

Data availability

Data will be made available on request.

References

Al-Ostaz, A., Jasiuk, I., 1997. Crack initiation and propagation in materials with randomly distributed holes. Eng. Fract. Mech. 58 (5–6), 395–420.

Amendola, A., Fortunato, A., Fraternali, F., Mattei, O., Milton, G.W., Seppecher, P., 2023a. Limit analysis of strut nets. Math. Mech. Solids 28 (8), 1760–1775.

Amendola, A., Mattei, O., Milton, G.W., Seppecher, P., 2023b. The obstacle problem in no-tension structures and cable nets. Proc. R. Soc. A 479 (2269), 20220229.

Angelillo, M.E., 2014. Mechanics of Masonry Structures, vol. 551, Springer.

Anjum, A., Hrairi, M., Aabid, A., Yatim, N., Ali, M., 2024. Civil structural health monitoring and machine learning: a comprehensive review. Fract. Struct. Integr. 18 (69), 43–59.

Baggio, C., Bernardini, A., Colozza, R., Corazza, L., 2014. Manuale Per La Compilazione Della Scheda Di 1 Livello Di Rilevamento Danno, Pronto Intervento E Agibilità Per Edifici Ordinari Nell'emergenza Post-Sismica (Aedes) - Seconda Edizione (In Italian). Protezione Civile, Presidenza del Consiglio dei Ministri.

Baggio, C., Bernardini, A., Colozza, R., Corazza, L., Della Bella, M., Di Pasquale, G., Dolce, M., Goretti, A., Martinelli, A., Orsini, G., et al., 2007. Field manual for post-earthquake damage and safety assessment and short term countermeasures (AeDES). In: European Commission–Joint Research Centre–Institute for the Protection and Security of the Citizen, EUR 22868.

Bagi, K., 2014. When Heyman's Safe Theorem of rigid block systems fails: Non-Heymanian collapse modes of masonry structures. Int. J. Solids Struct. 51 (14), 2696–2705.

Beatini, V., Royer-Carfagni, G., Tasora, A., 2019. Modeling the shear failure of segmental arches. Int. J. Solids Struct. 158, 21–39.

Bourahla, N., 2013. Equivalent static analysis of structures subjected to seismic actions. In: Encyclopedia of Earthquake Engineering. Springer, pp. 1–13.

Como, M., 2013. Statics of Historic Masonry Constructions, vol. 1, Springer.

De Filippo, M., Asadiabadi, S., Kuang, J., Mishra, D.K., Sun, H., 2023. AI-powered inspections of facades in reinforced concrete buildings. HKIE Trans. 30 (1), 1–14.

Heyman, J., 1995. The Stone Skeleton: Structural Engineering of Masonry Architecture. Cambridge University Press.

Katsigiannis, S., Seyedzadeh, S., Agapiou, A., Ramzan, N., 2023. Deep learning for crack detection on masonry façades using limited data and transfer learning. J. Build. Eng. 76, 107105.

Kumar, P., Sharma, A., Kota, S.R., 2021. Automatic multiclass instance segmentation of concrete damage using deep learning model. IEEE Access 9, 90330–90345.

Li, F., Luo, D., Niu, D., 2025. Data-intelligence driven methods for durability, damage diagnosis and performance prediction of concrete structures. Commun. Eng. 4 (1), 100.

Mishra, M., Lourenço, P.B., 2024. Artificial intelligence-assisted visual inspection for cultural heritage: State-of-the-art review. J. Cult. Herit. 66, 536–550.

Muñoz-Silva, E.M., Vasquez-Gomez, J.I., Merlo-Zapata, C.A., Antonio-Cruz, M., 2025. Binary damage classification of built heritage with a 3D neural network. Npj Herit. Sci. 13 (1), 124.

Pandolfi, A., Ortiz, M., 2012. An eigenerosion approach to brittle fracture. Internat. J. Numer. Methods Engrg. 92 (8), 694–714.

Pantoja-Rosero, B.G., Oner, D., Kozinski, M., Achanta, R., Fua, P., Pérez-Cruz, F., Beyer, K., 2022. TOPO-loss for continuity-preserving crack detection using deep learning. Constr. Build. Mater. 344, 128264.

Pratibha, K., Mishra, M., Ramana, G., Lourenço, P.B., 2023. Deep learning-based YOLO network model for detecting surface cracks during structural health monitoring. In: International Conference on Structural Analysis of Historical Constructions. Springer, pp. 179–187.

Ravichand, M., Kumar, R., Hazela, B., Suthar, T., 2022. Crack on brick wall detection by computer vision using machine learning. In: 2022 6th International Conference on Electronics, Communication and Aerospace Technology. IEEE, pp. 1017–1020.

Reis, H.C., Khoshelham, K., 2021. ReCRNet: a deep residual network for crack detection in historical buildings. Arab. J. Geosci. 14 (20), 2112.

Schmidt, B., Fraternali, F., Ortiz, M., 2009. Eigenfracture: an eigendeformation approach to variational fracture. Multiscale Model. Simul. 7 (3), 1237–1266.

Solomon Technology Corporation, 2025. Solomon SolVision. https://www.solomon-3d.com/products/solvision/. (Accessed 15 November 2025).

Wang, N., Zhao, Q., Li, S., Zhao, X., Zhao, P., 2018. Damage classification for masonry historic structures using convolutional neural networks based on still images. Comput.-Aided Civ. Infrastruct. Eng. 33 (12), 1073–1089.

Xu, Y., Li, Y., Zheng, X., Zheng, X., Zhang, Q., 2023. Computer-vision and machine-learning-based seismic damage assessment of reinforced concrete structures. Buildings 13 (5), 1258.